PRAMANA
— journal of
physics

© Indian Academy of Sciences

Vol. 67, No. 3
September 2006
pp. 467–475

Projected shell model study of neutron-deficient ^{122}Ce

RANI DEVI, B D SEHGAL and S K KHOSA
Department of Physics and Electronics, University of Jammu, Jammu 180 006, India
E-mail: rani_rakwal@yahoo.co.in

MS received 4 April 2006; revised 9 June 2006; accepted 7 July 2006

Abstract. The observed excited states of ^{122}Ce nucleus have been studied in the framework of projected shell model (PSM). The yrast band has been studied up to spin $26\hbar$. The first band crossing has been predicted above a rotational frequency of 0.4 MeV/$\hbar$ that corresponds to first backbending. The calculation reproduces the experimentally observed ground state band up to spin $14\hbar$. The electromagnetic quantities, transition quadrupole moments and g-factors are predicted and there is a need to measure these quantities experimentally.

Keywords. Projected shell model; band diagram; yrast energies; electromagnetic quantities.

PACS Nos 21.10.Re; 21.60.Cs; 21.10.Ky; 27.60.+j

1. Introduction

Recently, Smith *et al* [1] have communicated the existence of neutron-deficient ^{122}Ce and its excited states have been reported up to spin $14\hbar$. The band has been assigned to ^{122}Ce by detecting γ-rays in coincidence with evaporated charged particles and neutrons. The nucleus is believed to have large ground state quadrupole deformation (β_2) of value 0.35. In ^{122}Ce the experimental data do not extend beyond 0.4 MeV/$\hbar$ corresponding to the angular momentum state $14\hbar$. Aligned angular momenta have been studied and compared to Woods–Saxon cranking calculations and to the neighbouring cerium isotopes [2–5]. The $\pi(h_{11/2})^2$ alignment is not observed in ^{122}Ce until a rotational frequency of at least 0.4 MeV/$\hbar$ is reached. However, such alignments are observed in other cerium isotopes with $A \geq 124$ in the rotational frequency range from 0.3 to 0.4 MeV/$\hbar$. Since the experimental data on excitation energy spectra in ^{122}Ce are limited, one cannot comment on whether $\pi(h_{11/2})^2$ alignment and backbending phenomenon will occur in ^{122}Ce as it occurs in the neighbouring cerium isotopes, at a rotational frequency higher than 0.4 MeV/$\hbar$. However, it would be interesting to study these features on the basis

of theoretical results. This has been one of the motivating factors for the present work.

The purpose of the present paper is to investigate the structure of the ground state band in ^{122}Ce isotope and to see how satisfactorily the energy states of the ground state band with $J > 2$ are reproduced by taking β_2 as 0.35 from experiment as input. It is important to note that this value of β_2 has been extracted from the experimentally measured value of $E(2_1^+)$ energy state. Besides this, one would also like to find out what the theoretical results have to predict for the occurrence of $\pi(h_{11/2})^2$ alignment and backbending in this nucleus.

In the present study, projected shell model (PSM) [6] is employed to interpret the experimental data of ^{122}Ce. The PSM is a shell model truncated in the Nilsson single-particle basis, with pairing correlations incorporated into the basis by a BCS calculation for the Nilsson states. The Nilsson–BCS calculations provide us with a set of quasi-particle (qp) states that defines the qp vacuum. The deformed Nilsson states violate angular momentum which is recovered by an angular momentum projection technique [6]. Finally, a two-body shell model Hamiltonian is diagonalized in the projected space. Thus, the PSM has the main advantage of mean-field theories because it can easily build in the model the most important nuclear correlations. It solves the problem fully quantum mechanically and provides a good approximation to the exact shell model solution. In recent years, PSM has become quite successful in explaining a broad range of properties of deformed nuclei in various regions of the nuclear periodic table [7–10]. Very recently, the PSM has been systematically applied to the even–even proton-rich mass-80 and odd–odd proton-rich f-p-g shell nuclei [7] and the agreement between the PSM results and experimental data is found to be quite good.

2. The model

The detailed theory of PSM is given in a review article [6]. In this section, we give a brief outline of PSM. In PSM the shell model space is built by including 0-, 2- and 4-qp states:

$$|\phi_\kappa\rangle = \{|0\rangle, a^\dagger_{\nu 1}a^\dagger_{\nu 2}|0\rangle, a^\dagger_{\pi 1}a^\dagger_{\pi 2}|0\rangle, a^\dagger_{\nu 1}a^\dagger_{\nu 2}a^\dagger_{\pi 1}a^\dagger_{\pi 2}|0\rangle\}, \tag{1}$$

where $a^\dagger$s are the qp creation operators, νs(πs) denote the neutron(proton) Nilsson quantum numbers that run over the qp vacuum or zero quasi-particle state.

The Hamiltonian used in the present work is

$$\hat{H} = \hat{H}_0 - \frac{1}{2}\chi\sum_\mu \hat{Q}^\dagger_\mu \hat{Q}_\mu - G_{\rm M}\hat{P}^\dagger P - G_{\rm Q}\sum_\mu \hat{P}^\dagger_\mu \hat{P}_\mu, \tag{2}$$

where $\hat{H}_0$ is the spherical single-particle Hamiltonian which contains a proper spin–orbit force. The second, third and fourth terms represent quadrupole–quadrupole, monopole pairing and quadrupole pairing interactions, respectively. The strength of the quadrupole force χ is determined self-consistently by employing the quadrupole deformation parameter β_2. The monopole pairing strengths $G_{\rm M}$ used in the calculation are

$$G_{\rm M}^{\nu} = \left[19.60 - 15.70\frac{N-Z}{A}\right] A^{-1}, \quad G_{\rm M}^{\pi} = 19.60A^{-1}. \tag{3}$$

These strengths are taken from ref. [8] with a scaling factor of 1.1. The motivation for including the quadrupole pairing term in the Hamiltonian has been to take account of pairing effects, acting between like nucleons coupled to spin 2. It may be considered as a correction to the monopole pairing force. It reduces the strength of the Coriolis force and it is also responsible for reproducing correct band crossing in doubly even rare-earth nuclei [10]. In the present work, the strength of the quadrupole pairing force $G_{\rm Q}$ is assumed to be proportional to $G_{\rm M}$. The value of the proportionality constant has been adjusted to get the best representation of experimental observation. For ^{122}Ce, its value has been fixed as 0.20 that is comparable to the value taken by Hara and Sun [6,10] for the PSM calculations of the lighter part of rare-earth region.

The PSM wave function is written as a linear combination of the angular momentum projected states and is given by

$$|\sigma, IM\rangle = \sum_{K,\kappa} f_{\kappa}^{\sigma} \hat{P}_{MK}^{I} |\phi_{\kappa}\rangle. \tag{4}$$

The index σ labels the states with same angular momentum and κ the basis states. P_{MK}^{I} is angular momentum projection operator and f_{κ}^{σ} are the weights of the basis states κ.

The eigenvalue equation of the PSM for given spin I takes the form [6]

$$\sum_{\kappa'} (H_{\kappa\kappa'} - E_{\sigma} N_{\kappa\kappa'}) f_{\kappa'}^{\sigma} = 0. \tag{5}$$

The angular momentum-projected wave functions are the laboratory functions, and can thus be used to compute the observables. In the present work, we have computed the electromagnetic properties using PSM approach.

The reduced transition probabilities $B(EL)$ from the initial state $(\sigma_{\rm i}, I_{\rm i})$ to the final state $(\sigma_{\rm f}, I_{\rm f})$ are given by [9]

$$B(EL, I_{\rm i} \longrightarrow I_{\rm f}) = \frac{e^2}{(2I_{\rm i}+1)} |\langle \sigma_{\rm f}, I_{\rm f} \| \hat{Q}_L \| \sigma_{\rm i}, I_{\rm i} \rangle|^2, \tag{6}$$

where the reduced matrix element is given by [9]

$$\begin{aligned}
\langle \sigma_{\rm f}, I_{\rm f} \| \hat{Q}_L \| \sigma_{\rm i}, I_{\rm i} \rangle = & \sum_{\kappa_{\rm i}, \kappa_{\rm f}} f_{\kappa_{\rm i}}^{\sigma_{\rm i}} f_{\kappa_{\rm f}}^{\sigma_{\rm f}} \sum_{M_{\rm i}, M_{\rm f}, M} (-)^{I_{\rm f} - M_{\rm f}} \\
& \times \begin{pmatrix} I_{\rm f} & L & I_{\rm i} \\ -M_{\rm f} & M & M_{\rm i} \end{pmatrix} \langle \phi_{\kappa_{\rm f}} | \hat{P}_{K_{\kappa_{\rm f}} M_{\rm f}}^{I_{\rm f}} \hat{Q}_{LM} \hat{P}_{K_{\kappa_{\rm i}} M_{\rm i}}^{I_{\rm i}} | \phi_{\kappa_{\rm i}} \rangle \\
= & \, 2 \sum_{\kappa_{\rm i}, \kappa_{\rm f}} f_{\kappa_{\rm i}}^{\sigma_{\rm i}} f_{\kappa_{\rm f}}^{\sigma_{\rm f}} \sum_{M', M''} (-)^{I_{\rm f} - K_{\kappa_{\rm f}}} (2I_f + 1)^{-1} \\
& \times \begin{pmatrix} I_{\rm f} & L & I_{\rm i} \\ -K_{\kappa_{\rm f}} & M' & M'' \end{pmatrix} \int {\rm d}\Omega D_{M'' K_{\kappa_{\rm i}}}(\Omega) \\
& \times \langle \phi_{\kappa_{\rm f}} | \hat{Q}_{LM'} \hat{R}(\Omega) | \phi_{\kappa_{\rm i}} \rangle.
\end{aligned} \tag{7}$$

The transition quadrupole moment $Q_{\rm t}(I)$ is related to the $B(E2)$ transition probability through

$$Q_t(I) = \left(\frac{16\pi}{5}\frac{B(E2, I \to I-2)}{\langle IK20|I-2K\rangle}\right)^{1/2}. \tag{8}$$

In the calculations, we have used the effective charges of $1.5e$ for protons and $0.5e$ for neutrons.

The gyromagnetic factors (g-factors), $g(\sigma, I)$, $g_\pi(\sigma, I)$ and $g_\nu(\sigma, I)$ are defined by [9]

$$g(\sigma, I) = \frac{\mu(\sigma, I)}{\mu_N I} = g_\pi(\sigma, I) + g_\nu(\sigma, I) \tag{9}$$

with $g_\tau(\sigma, I)$, $\tau = \pi$, ν given by

$$g_\tau(\sigma, I) = \frac{1}{\mu_N[I(I+1)]^{1/2}} \times[g_l^\tau \langle\sigma, I\|\hat{J}^\tau\|\sigma, I\rangle + (g_s^\tau - g_l^\tau)\langle\sigma, I\|\hat{S}^\tau\|\sigma, I\rangle] \tag{10}$$

and $\mu(\sigma, I)$ is the magnetic moment of a state (σ, I). In our calculations, the following standard values of g_l and g_s have been taken: $g_l^\pi = 1$, $g_l^\nu = 0$, $g_s^\pi = 5.586 \times 0.75$, and $g_s^\nu = -3.826 \times 0.75$. g_s^π and g_s^ν are damped by a factor of 0.75 from the free nucleon values to account for the core-polarization and meson-exchange current corrections [11].

3. Results and discussion

In the present calculation the Nilsson parameters are taken from ref. [12] and the calculations are performed by considering three major shells ($N = 3$, 4 and 5) for both protons and neutrons. The basis deformation β_2 is taken from ref. [1] as $\beta_2 = 0.35$ and $\beta_4 = -0.013$ [13]. The intrinsic states within the chosen energy window around the Fermi surface give rise to the size of the basis space $|\phi_\kappa\rangle$, in eq. (4) of the order of 67. In figure 1, the band diagram [10] which gives the projected energies for the configurations close to the Fermi surface is displayed. For each band, its quasi-particle configuration is marked. In our calculations we obtain 67 bands but in figure 1, only the lowest proton and neutron bands are plotted whose weight factors are $\geq$0.10. These bands have dominant contribution to the yrast band of ^{122}Ce. From figure 1, it is seen that between spin $I = 16 - 18\hbar$, three 2-qp proton bands cross the ground state band and come down in energy and become yrast. These bands consist of $\pi h_{11/2}[1/2, 3/2]$, $\pi h_{11/2}[3/2, 5/2]$ with $K = 1$ and $\pi h_{11/2}[3/2, 3/2]$ with $K = 0$ configurations. The neutron 2-qp band consisting of configuration $\nu h_{11/2}[5/2, 7/2]$ with $K = 1$, after crossing the ground state band goes up along with it and never appears as yrast. Thus, the yrast states above spin $16\hbar$ are a superposition of three proton 2-qp bands. The 4-qp bands consisting of a pair of protons and a pair of neutrons are not displayed in figure 1 as these bands do not contribute to the yrast band up to spin $I = 26$ and lie higher in energy.

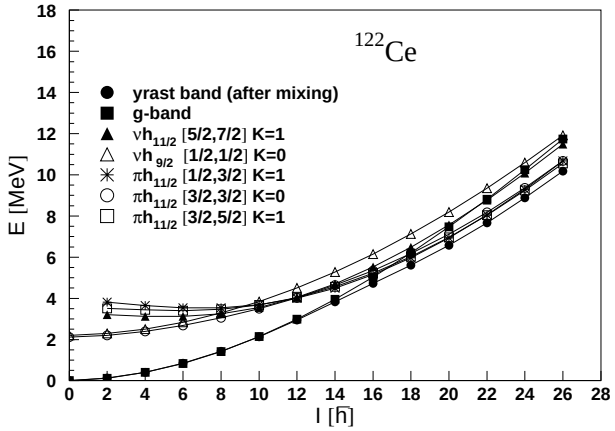

Figure 1. Band diagram (bands before configuration mixing) and the yrast band (the lowest band after configuration mixing) for ^{122}Ce. Only the important lowest-lying bands in each configuration are shown.

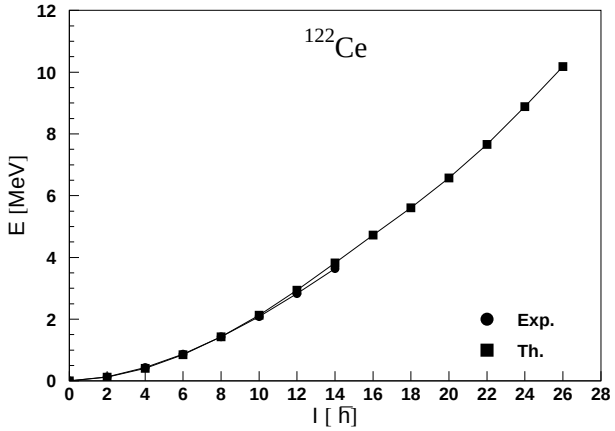

Figure 2. Comparison of the calculated energies $E(I)$ of the yrast band with experimental data of ^{122}Ce. The calculated yrast band consists of the lowest states after diagonalization at each angular momentum I.

In figure 2, we have compared the calculated yrast band that consists of the lowest energies after diagonalization at each spin with available data. These values are also displayed in figure 3 in a sensitive plot of moment of inertia as a function of the square of the rotational frequency. Figures 2 and 3 show good agreement with the experimental data. Based on PSM results, the yrast band of ^{122}Ce can be assigned the following configurations: At low spin, the yrast band is built up on the qp vacuum (0-qp) configuration. The 0-qp configuration is dominant up to spin $16\hbar$. Above spin $16\hbar$, the yrast band is a superposition of three 2-qp proton configurations $\pi h_{11/2}[1/2, 3/2]$, $K = 1$; $\pi h_{11/2}[3/2, 5/2]$, $K = 1$ and $\pi h_{11/2}[3/2, 3/2]$, $K = 0$. In table 1, the weight factors obtained from the shell model

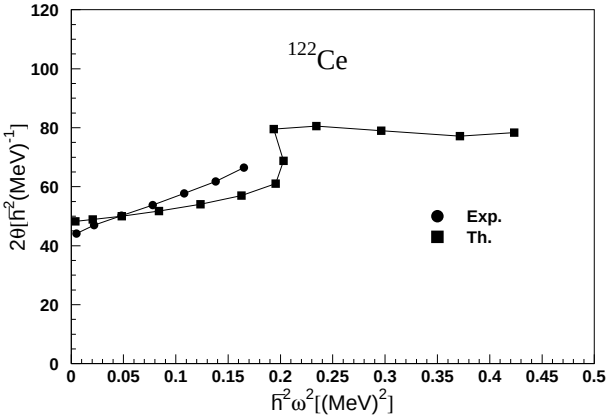

Figure 3. Comparison of the calculated moment of inertia 2θ with experimental data as a function of square of rotational frequency ω^2. These quantities are defined as $2\theta = \frac{2I-1}{\omega}$, $\omega = [E(I) - E(I-2)]/2$.

diagonalization, corresponding to these configurations are presented. The weight factors of $\pi h_{11/2}[3/2, 5/2]$, $K = 1$ and $\pi h_{11/2}[3/2, 3/2]$, $K = 0$ configurations are $\geq$0.20. It is observed from the calculated results presented in figure 3 that there is occurrence of backbending around spin $16\hbar$ in ^{122}Ce that needs to be verified experimentally.

In figures 4 and 5, the $Q_{\rm t}$ values and $B(E2)$ values are displayed as a function of spin I. It is seen from these figures that $Q_{\rm t}$ and $B(E2)$ values show a reduction in their values at spin $I = 16$. The reduction in these values may be thought to be associated with the first band crossing that leads to backbending phenomena. Above spin $16\hbar$, these values are nearly constant up to spin $24\hbar$.

In figure 6, the calculated results on gyromagnetic (g) factors are displayed as a function of spin (I). A proton alignment, produces an increase of $g_{\rm p}$, while $g_{\rm n}$ should change very little. The overall effect is an increase of the total g-factor. From figure 6, it can be seen that $g_{\rm n}$ and $g_{\rm p}$ remain almost constant up to spin $14\hbar$. Above spin $14\hbar$, we observe an increase in total g-factor. This can be interpreted to be due to $h_{11/2}$ proton alignment. In figure 6, we have also plotted the rigid body value of g-factor. It is observed from this figure that at spin $I = 14$, the calculated value of g-factor is exactly equal to the rigid body value. Above spin $20\hbar$, the g-factors are almost constant. Unfortunately, there is no experimental data to compare with.

4. Conclusions

In summary, the experimental data of ground state band in ^{122}Ce has been described in the framework of PSM. The calculated energy levels agree well with the observed ground state band. The first backbending is predicted due to the crossing of proton 2-qp bands around spin $16\hbar$. After the band crossing, the yrast energies are predicted to be a superposition of three proton 2-qp bands up to spin $26\hbar$.

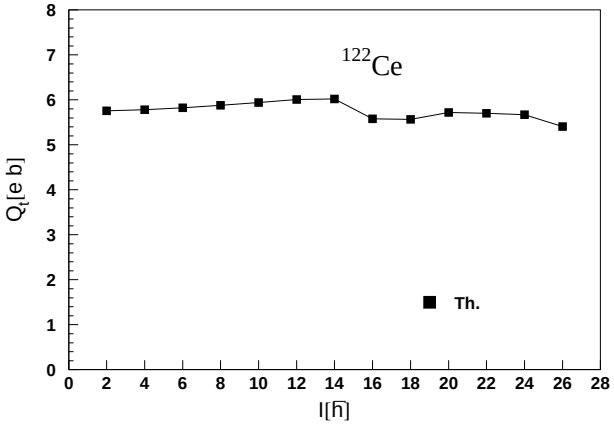

Figure 4. Predicted transition quadrupole moments $Q_{\rm t}$ as a function of the angular momentum for the yrast band in ^{122}Ce.

Table 1. Predicted configurations and weight factors for energy states of yrast band in ^{122}Ce.

Spin I ($\hbar$)	Configurations	Weight factors
0	0-qp	0.954
2	0-qp	0.955
4	0-qp	0.956
6	0-qp	0.956
8	0-qp	0.950
10	0-qp	0.934
12	0-qp	0.897
14	0-qp	0.813
16	0-qp	0.558
	$\pi h_{11/2}$[3/2,5/2], $K=1$	0.149
	$\pi h_{11/2}$[3/2,3/2], $K=0$	0.118
18	0-qp	0.218
	$\pi h_{11/2}$[3/2,5/2], $K=1$	0.252
	$\pi h_{11/2}$[3/2,3/2], $K=0$	0.218
20	$\pi h_{11/2}$[3/2,5/2], $K=1$	0.234
	$\pi h_{11/2}$[3/2,3/2], $K=0$	0.255
	$\pi h_{11/2}$[1/2,3/2], $K=1$	0.108
22	$\pi h_{11/2}$[3/2,5/2], $K=1$	0.261
	$\pi h_{11/2}$[3/2,3/2], $K=0$	0.238
	$\pi h_{11/2}$[1/2,3/2], $K=1$	0.106
24	$\pi h_{11/2}$[3/2,5/2], $K=1$	0.249
	$\pi h_{11/2}$[3/2,3/2], $K=0$	0.294
	$\pi h_{11/2}$[1/2,3/2], $K=1$	0.100
26	$\pi h_{11/2}$[3/2,5/2], $K=1$	0.219
	$\pi h_{11/2}$[3/2,3/2], $K=0$	0.287
	$\pi h_{11/2}$[1/2,3/2], $K=1$	0.100

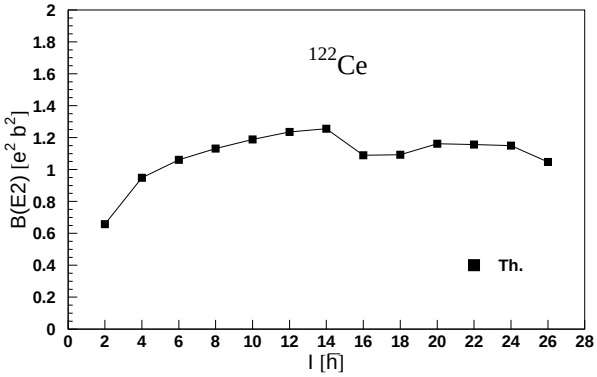

Figure 5. Predicted reduced transition probabilities $B(E2)$ as a function of the angular momentum for the yrast band in ^{122}Ce.

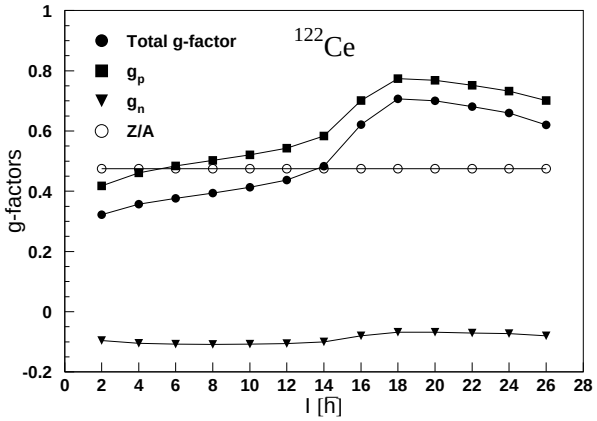

Figure 6. Predicted g-factors as a function of angular momentum for the yrast band in ^{122}Ce. Here $g_{\rm p}(g_{\rm n})$ denotes proton(neutron) contribution to g-factors and Z/A is rigid body value.

Electromagnetic properties in the yrast band have been studied with predictions made for the $Q_{\rm t}$, $B(E2)$ and g-factor values. These predictions have to be verified experimentally.

Acknowledgements

The authors would like to thank Prof. J A Sheikh for valuable discussions about their results. One of the authors (RD) acknowledges Department of Science and Technology, New Delhi for financial support.

References

[1] J F Smith *et al, Phys. Lett.* **B625**, 203 (2005)

[2] J F Smith *et al, Phys. Rev.* **C69**, 034339 (2004)
[3] A N Wilson *et al, Phys. Rev.* **C63**, 054307 (2001)
[4] E S Paul *et al, Nucl. Phys.* **A676**, 32 (2000)
[5] D M Todd, R Aryaeinejad, D J G Love, A H Nelson, P J Nolan, P J Smith, P J Twin, *J. Phys.* **G10**, 1407 (1984)
[6] K Hara and Y Sun, *Int. J. Mod. Phys.* **E4**, 637 (1995)
[7] R Palit, J A Sheikh, Y Sun and H C Jain, *Nucl. Phys.* **A686**, 141 (2001); *Phys. Rev.* **C67**, 014321 (2003)
[8] Y Sun and M Guidry, *Phys. Rev.* **C52**, R2844 (1995)
[9] Y Sun and J L Egido, *Nucl. Phys.* **A580**, 1 (1994)
[10] K Hara and Y Sun, *Nucl. Phys.* **A529**, 445 (1991) and references cited therein
[11] B Castel and I S Towner, *Modern theories of nuclear moments* (Clarendon Press, Oxford, 1990)
[12] J-Y Zhang, N Xu, D B Fossan, Y Liang, R Ma and E S Paul, *Phys. Rev.* **C39**, 714 (1989)
[13] P Moller, J R Nix, W D Myers and W J Swiatecki, *At. Data Nucl. Data Tables* **59**, 185 (1995)